Co-funded by the European Union

Project No : 101094628

Project Number:
101094628

Project Acronym:
ESSnuSBplus

Call Identifier:
HORIZON-INFRA-2022-DEV-01

Project Full Title:
Study of the use of the ESS facility to accurately measure the neutrino cross-sections for ESSnuSB leptonic CP violation measurements and to perform sterile neutrino searches and astroparticle physics

Start date of project: 2023-01-01
Duration: 4 years
Milestone title: Final estimation of the pion beam (WP3+)
Due delivery date: 2025-12-31
Actual delivery date: 2025-12-31
Organisation name of lead contractor for this milestone: Centre National de la Recherche Scientifique (CNRS)

Project co-funded by the European Commission within Horizon Europe Framework Programme		
Dissemination level		
PU	Public	X
CO	Confidential, only for members of the consortium (including the Commission Services)	
EU-RES	Classified information: RESTREINT UE (Commission Decision 2005/444/EC)	
EU-CON	Classified information: CONFIDENTIEL UE (Commission Decision 2005/444/EC)	
EU-SEC	Classified information: SECRET UE (Commission Decision 2005/444/EC)	

Milestone number	M22
Milestone name	Final estimation of the pion beam
Type of document	Report
Work Package	WP3: Target Station & Pion Extraction
Lead Contractor	CNRS, France
Lead Coordinators	UU Sweden, CERN Geneva

Authors' name	Organisation	Email
Jorge Aguilar	ESSB	jaguilar@essbilbao.org
Eric Baussan	CNRS	eric.baussan@iphc.cnrs.fr
Elian Bouquerel	CNRS	elian.bouquerel@iphc.cnrs.fr
Ting W. Choi	Uppsala University	ting.choi@physics.uu.se
Ilias Efthymiopoulos	CERN	Ilias.Efthymiopoulos@cern.ch
Caren Hagner	UHH	caren.hagner@desy.de
Julien Hiegel	CNRS	julien.hiegel@iphc.cnrs.fr
Miguel Magán	ESSB	mmagan@essbilbao.org
Maja Olvegård	Uppsala University	maja.olvegard@physics.uu.se
Pascal Poussot	CNRS	pascal.poussot@iphc.cnrs.fr
Cedric Schwab	CNRS	cedric.schwab@iphc.cnrs.fr
Fernando Sordo Baldin	ESSB	fsordo@essbilbao.org
Tamer Tolba	UHH	tamer.tolba@uni-hamburg.de
Max Topp-Mugglestone	CERN	max.emil.topp-mugglestone@cern.ch
Jacques Wurtz	CNRS	jacques.wurtz@iphc.cnrs.fr
Valeria Zeter	CNRS	valeria.zeter@iphc.cnrs.fr

Abstract

The ESSnuSB+ project appears as intermediate phase of the Long Baseline neutrino superbeam project aims to measure the CP violation parameter. In this project, the generation of a neutrino superbeam is realized by the decay of muons circulating in a race ring. The target station has to be equipped with additional elements constituting the Target to Ring transfer line (T2R) which allow to select the pions in the energy range defined by the physics reaches from the production stage to feed the Low Energy NuSTORM racetrack ring. In this document, the main elements from the pion production will be recalled and the design of the Target To Ring (T2R) elements will be presented.

List of abbreviations The following table presents by alphabetical order, the acronyms used in this milestone:

Abbreviation	Description
ESS	European Spallation Source
ESSnuSB	European Spallation Source Neutrino Super-Beam
nuSTORM	neutrinos from STOred Muons
LEnuSTORM	Low Energy neutrinos from STOred Muons
LEMMOND	Near Detector for the LEnuSTORM and MOnitored beams
BD	Beam Dump
LADM	Large-Aperture Dipole Magnet
T2R	Target to Ring
WP	Work Package
LBL	Long-baseline neutrino beam
END	ESSnuSB Near Detector

Contents

1 Introduction

Because the production and the accurate determination of the pion beam are crucial factors in the production of the final neutrino beam, the main objective of the ESSnuSBplus target station is to produce a well-defined pion beam to produce a neutrino beam with the desired momentum range required by the experiment's physics case. This milestone is dedicated to studying the baseline beam profile, momentum range, and spatial distribution of the pion beam produced by the ESSnuSBplus target station. This study uses the ESSnuSB pack-bed target, which consists of titanium spheres with a diameter of 3 mm that are housed in a Ti canister with a diameter of 3 cm and a length of 78 cm. This target will be hit by a proton beam with an energy of 2.5 GeV and a power of 1.25 MW. The produced pions will be focused to the forward direction by a MiniBooNE-like horn. Furthermore, this study discusses the design of the target-to-ring transfer line, which will transfer the focused pion beam from the production area after the focusing dipole magnet to the Low-Energy nuSTROM (LEnuSTORM) racetrack ring.

2 Pion Beam Production

The ESSnuSB Target Station will host in the phase 2 of the project one magnetic horn converting a 2.5 GeV proton beam with 1.25 MW beam power. The pion production has been optimized regarding the physics performances of the experiment [1]. In the following, the important points of the development will be recalled regarding the horn and the Large-aperture Dipole Magnet (LADM).

2.1 Hadronic Collector

The ESSnuSB+ horn's design is based on the previous project aimed for at CP violation measurment and has been re-optimized regarding the ESSnuSB+ physics requirements. The produced pions are focussed by one magnetic horn and selected by a Large Aperture Dipole Magnet (LADM) located downstream of the horn. To protect this magnet against a high level of radiations a shielding has been implemented as shown in Figure 1 (Left).

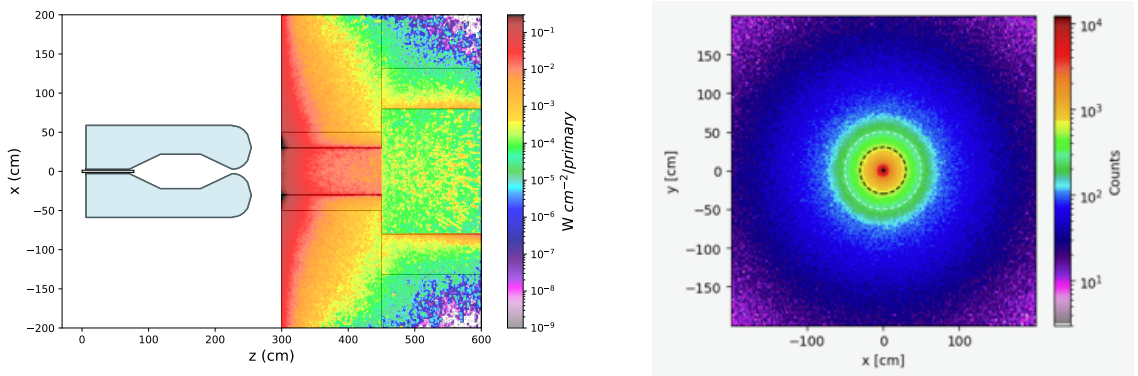

Figure 1: Power density deposition in the collimator and the magnet (Left) Spatial distribution in the transverse plane at the dipole level (Right).

The dimensions of the shielding imposes a important reduction pions fluxes whose the spatial distribution is shown in Figure 1 (Right). The collimated pions are deviated by a dipole magnet located just after whose the main feature are discussed in the next section.

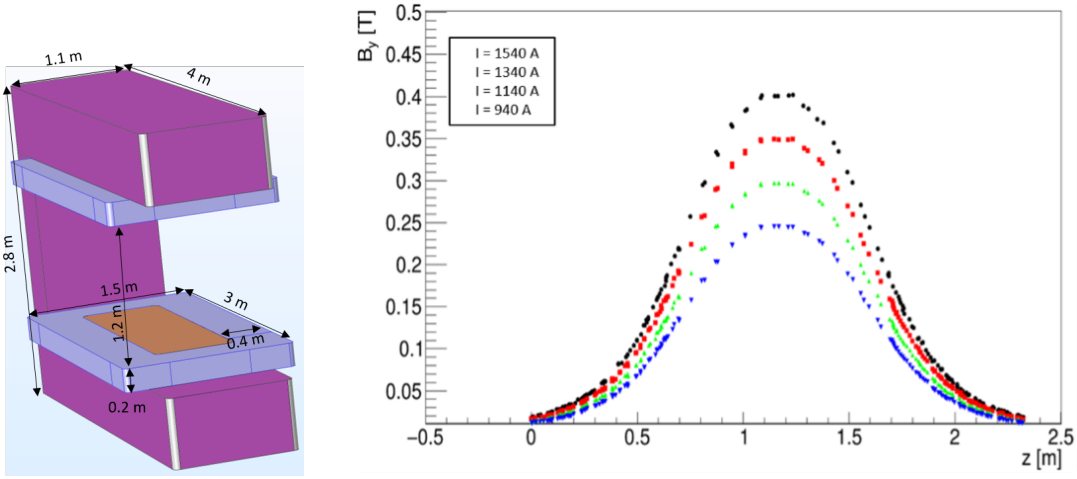

Figure 2: LADM design COMSOL models. Geomtry (Left). B_y component of the magnetic field at the central trajectory and for $y = 0$ for B field at y = 0 cm along the pion beam (z-) axis at different coil current values (Right).

2.2 Large-aperture Dipole Magnet (LADM)

The design of the LADM plays a key role as the first element in defining the pion beam profile and energy that will be further fed to the LEnuSTORM ring via the transfer-line. It must provide sufficient magnetic strength to deflect the secondary pions from the target-horn system with the defined momentum while having a sufficiently large aperture to avoid being a limiting factor for the pion flux. Furthermore, it must be robust enough to withstand the radiation levels in the region produced by the 1.25 MW primary proton beam. Table 1 summarizes the key parameters of the baseline design of the LADM.

Table 1: Key design parameters for the LADM corresponding to the baseline design of T2R.

Parameter	**Unit**	**Value**
Bending angle (h-plane)	[deg]	29.5
Pion momentum	[GeV]	0.7
Integral field Bdl	[T m]	1.2022
Beam size ($1\,\sigma_{x,y}$)	[cm]	20
Aperture [H×V]		
one-sigma	[cm]	$[70 \times 40]$
two-sigma	[cm]	$[100 \times 80]$

COMSOL Multiphysics framework [2] is used to simulate the electrodynamic behaviour of the LADM. Figure 2 shows the COMSOL 3D model of the magnet structure, which is used in this study. The final design will be tailored to meet the parameters listed in Table 1. It will also include an optimized coil structure to ensure a uniform magnetic field over an extended region inside the magnet core, as well as measures to mitigate fringe fields arising from the large aperture.

Figure 2 illustrates the Y-component of the magnetic field (B_y) along the central trajectory $(y = 0)$ on the pion beam (z) axis for various coil current settings. A field strength of $B_y = 0.4\,\mathrm{T}$ is achieved with a coil current of 1540 A. While the baseline design assumes a maximum field of $B_{y,max} = 1.0\,T$ as described in the previous sections, if shown to be not possible, a more practical compromise would be $B_{y,max} = 0.8\,\mathrm{T}$, corresponding to a dipole length of approximately 1.5 m.

3 Pion Transfer Line Design

Pions downstream of the horn must be transported and injected into the LEnuSTORM decay ring. The position of the injection point is determined by the location of the LEnuSTORM production straight, which is constrained in that it must point directly towards the Long Baseline Near Detector (END) - which is located along the axis of the decay tunnel, coaxial to the target/horn system - without intersecting the decay tunnel or its shielding. The geometry of this is depicted in Figure 3.

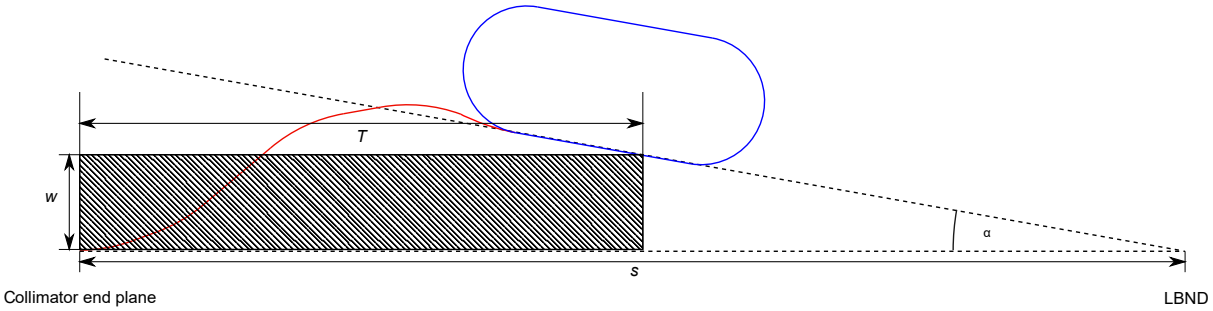

Figure 3: Geometry diagram showing the decay tunnel and shielding (shaded area), pion transfer line (red), and LEnuSTORM ring (blue). The elements are not depicted to scale.

3.1 Layout

With knowledge of the width of the decay tunnel of the ESSnuSB Target Station and its shielding, the minimum angle α to avoid intersection of the LEnuSTORM ring with the decay tunnel can be computed as

$$\tan\alpha = \frac{w}{s-T}, \tag{1}$$

in which w is the half-width of the decay tunnel and associated shielding, assumed to be 8 m, T is the length of the decay tunnel, and s is the position of the END with respect to the target station.

The angle of the pion beam at the end of the transfer line with respect to the axis of the decay tunnel is then determined by the angle of the production straight α and the angle of the momentum-offset optics of the stochastic injection section of the LEnuSTORM ring (Figure 4). The total bending angle of the transfer line must be equal to the sum of these angles.

3.2 Transfer line concept

The second constraint on the transfer line is that the optics of the line must transform the Courant-Snyder parameters of the output distribution from the horn (computed from the covariance matrix) to match those at the input of the stochastic injection section. The latter are computed by evaluating the periodic optics of the production straight and then propagating them in reverse through the stochastic injection section (illustrated in Figure 4).

The first part of this is to ensure the matching of dispersion; this is zero at the horn output, and must be zero in the production straight. As an initial approach, the transfer line is designed with two independent closed-dispersion arcs and a short straight with zero first-order dispersion. This means that dispersion can be considered (at first order) in the optimisation as being confined to the arc sections, meaning that only the arc quadrupoles need to be tuned to suppress dispersion and the quadrupoles in the straight can be tuned to match the horizontal beta and alpha functions. Furthermore, by using two identical copies of the LADM, the total

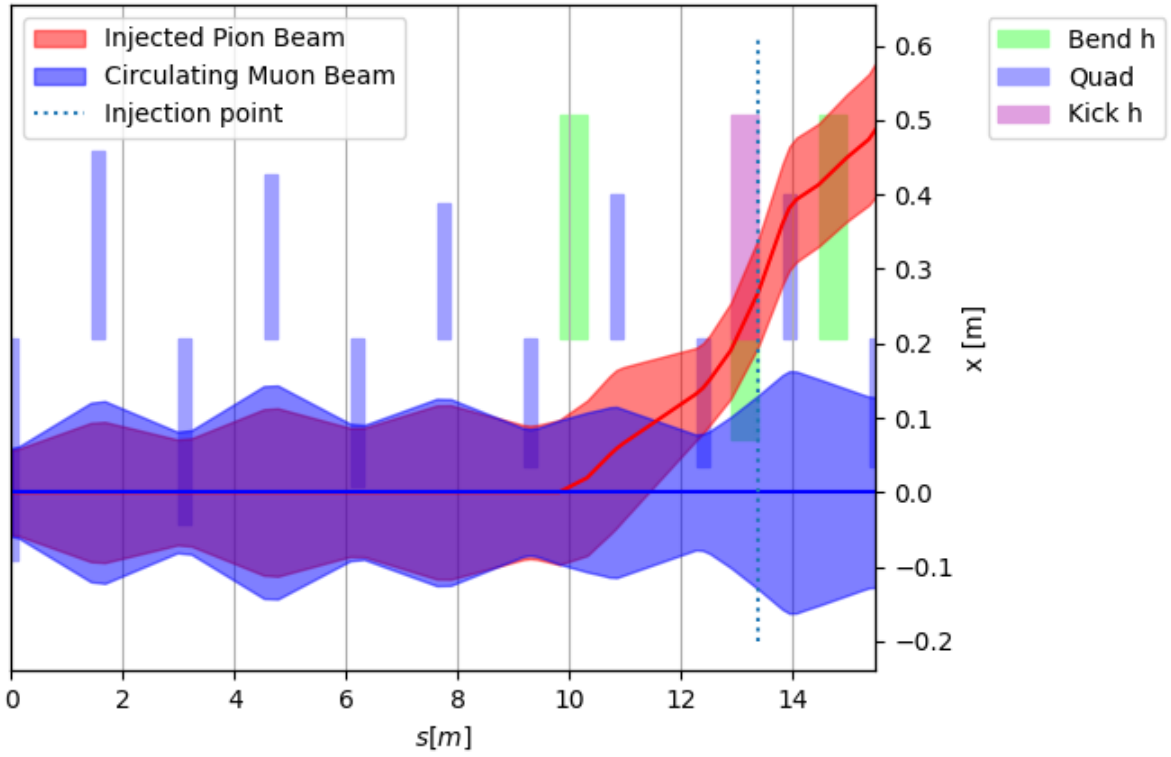

Figure 4: Beam envelopes for the pion and muon beams propagating in reverse direction from the production straight into the injection arc. Initial parameters of both beams are determined from the periodic optics of the lattice, with the emittance of the pion beam at the nominal value used elsewhere in this docuument, and the emittance of the muon beam taken to be 3 mm. The momentum spread in each case is assumed to be $\pm 10\%$. The central muon momentum is the reference momentum of 600 MeV/c selected for the LEnuSTORM ring and the central pion momentum is 1050 MeV/c. The downstream plane of the septum magnet (dashed vertical line) is considered to be the injection point and the point at which the transfer line connects to the ring. The pion optics to the right of this in the figure are not considered relevant as pions do not traverse this section of the ring.

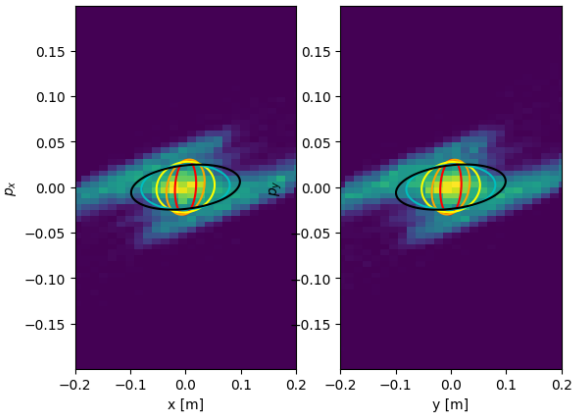

Figure 5: Initial phase space of the pion beam within the assumed ±10% momentum acceptance. The coloured ellipses represent the Courant-Snyder ellipses corresponding to fractions of the beam with the lowest radial distance from the axis as follows: red, 10%; orange, 25%; yellow, 50%; cyan, 90%; black, 100%.

bending angle of the first arc of the line can be increased, meaning that the required lateral distance through the shielding can be traversed with a shorter total length of the transfer line. The bending angle of the first arc is then fixed by the parameters of the LADM, whilst the second arc needs a bending angle equal to this value plus the additional component from the angular offset of the production straight, and that from the deflection of the pion beam as it travels through the stochastic injection section (α_π).

3.3 Computation of Initial Parameters

The simulation performed under FLUKA [3, 4] whose main results are reported in section 2.1 and was used to obtain the pion distribution on the upstream plane of the collimator. The corresponding distribution was then transformed into the accelerator (Frenet-Serret) coordinate system relevant to the beamline, with a reference momentum P_0 chosen at 1050 MeV/c. The particles were then propagated through the collimator using an Xsuite [5] simulation, and the resulting distribution was used to compute Courant-Snyder parameters.

Table 2: Courant-Snyder parameters for different beam cuts downstream of the collimator. Due to the axial symmetry of the distribution, equivalent values are assumed for both planes.

	ϵ [m]	β [m]	α
10%	5.7×10^{-4}	0.64	0.14
25%	1.0×10^{-3}	1.16	0.21
50%	1.5×10^{-3}	1.89	0.09
90%	2.0×10^{-3}	3.25	0.09
100%	2.4×10^{-3}	4.10	0.25

The distribution was sliced to select given proportions of particles with the lowest radial distance from the origin of the coordinate system, within the momentum range of ±10%. The computed Courant-Snyder parameters for each subselection of the distribution are displayed in Table 2, with the phase space distribution and relevant ellipses displayed in Figure reffig:horn-dist. It is evident that the non-uniform phase space produced by the horn results in radically different optical parameters depending on the fraction of the beam selected. For the purposes of an initial optimisation of the linear optics, we elect to focus the design on

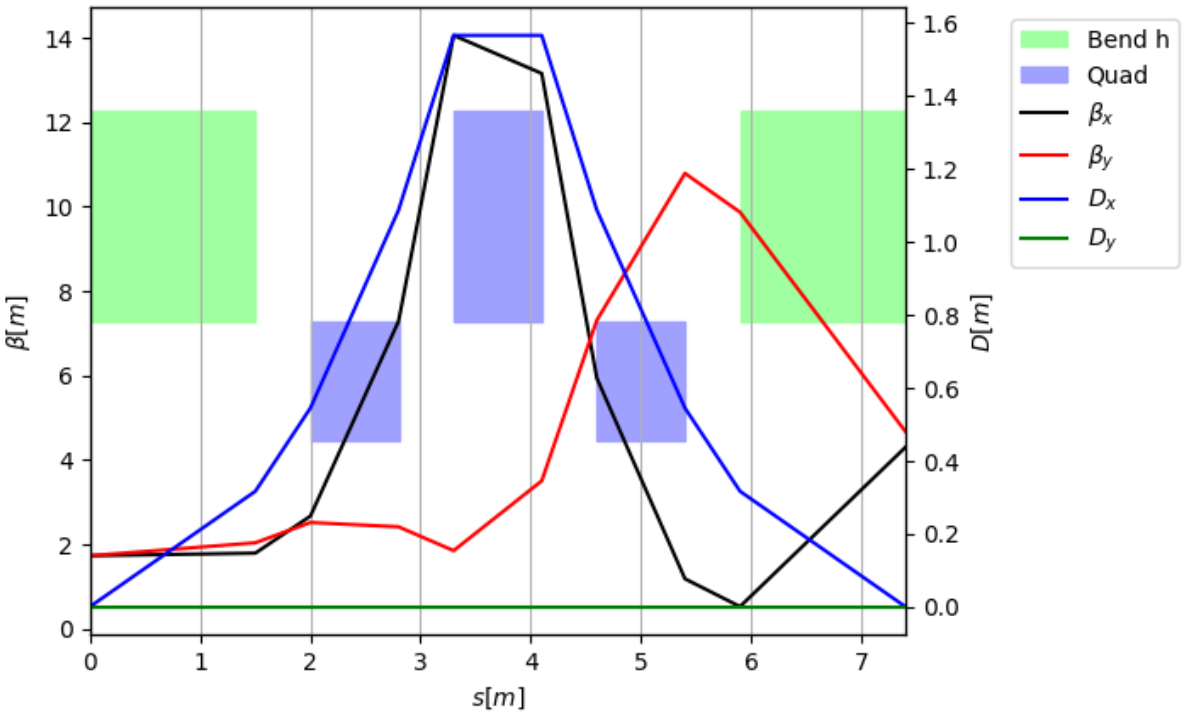

Figure 6: Linear optics of the Target Station Arc of the Transfer Line

transportation of the dense beam core, and select as the baseline input parameters those corresponding to the distribution of the innermost 50% of the particles.

3.4 Design of Target Station Arc

The design of the first arc of the transfer line is constrained by the limited fields of the LADM. As mentioned previously, the use of two dipoles in the first arc enables a larger bending angle than would otherwise be achieved with a single dipole, and the use of two dipoles with similar properties enables exploitation of the arc's symmetry to suppress dispersion (by tuning the phase advance of of the intermediate optics to be equal to π in the horizontal plane).

The LADM is modelled in XSuite as a Bend element with an edge angle corresponding to the overall bending angle of the element (i.e. a rectangular element with an entrance plane perpendicular to the beam axis). The k_0 value (inverse of the radius of curvature) is set by assuming a dipole field of 0.79 T and computing the magnetic rigidity of the beam. For the initial design study, the second dipole of the arc is considered as a mirror-symmetric copy (about the midpoint of the arc), but manufacture costs could be optimised by reduction of the aperture of this second dipole owing to its positioning outside of the high-radiation target environment.

A horizontally-focussing (F) quadrupole must be included to control the horizontal phase advance and suppress dispersion. As the dispersion grows linearly downstream of the dipole, this quadrupole should be positioned as close as possible to the dipole. However, a horizontally-focussing quadrupole is necessarily defocussing in the vertical plane; vertically-focussing (D) quadrupoles must also be included to keep the beam constrained in both planes. To maintain the required symmetry for the dispersion suppression, we arrive at the triplet configuration shown in Figure 6. To minimise overall beam size and maximise acceptance, the quadrupoles must be positioned as tightly as possible with respect to each other, and as close to the dipoles as geometric and shielding constraints permit. The study of shielding between the dipole and

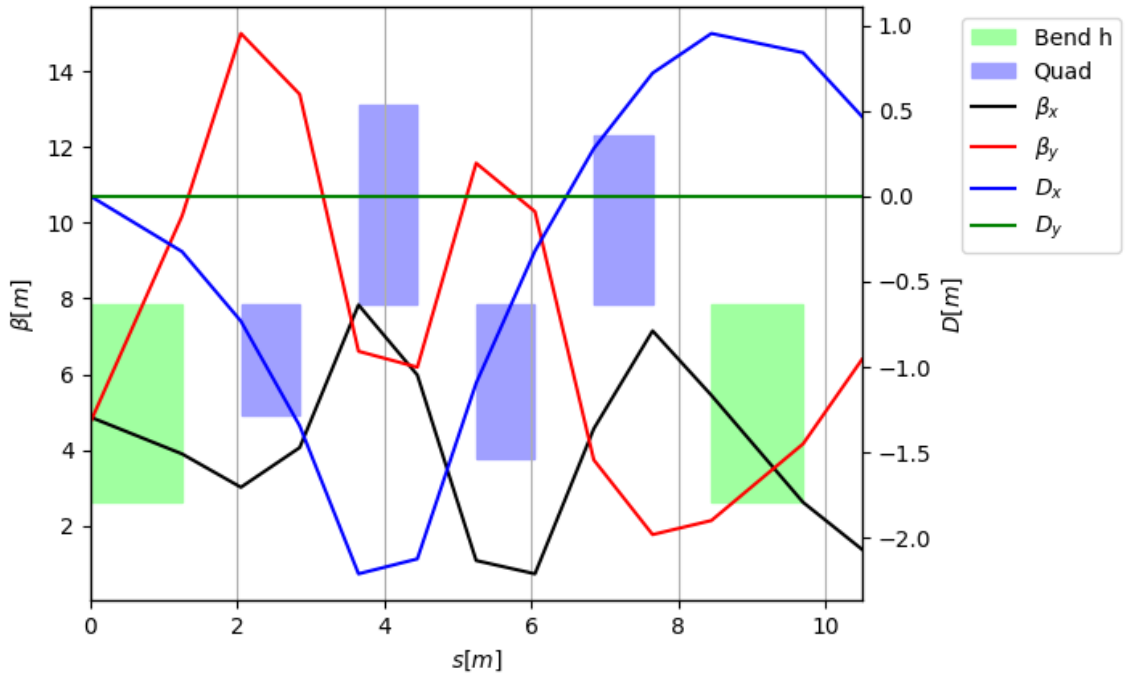

Figure 7: Optics of the injection-matching arc for the transfer line. The right hand side represents the position of the injection septum.

first quadrupole and effects of shielding on the design of this arc will be the subject of further simulation in FLUKA. The quadrupole coefficients for the arc k_{1F} and k_{1D} are set such that dispersion and its first derivative at the end of the dipole are equal to zero.

3.5 Design of Injection-Matching Arc

The overall bending angle of the two dipoles in the second arc is given by the sum of the angle of the pion beam at the injection point and the total angle of the first arc, which was determined based on field constraints. For these dipoles we assume a more conservative aperture will allow a higher dipole field, which we assume to be 1.5 T based on limits for normal-conducting magnets [6]. As this line is not a closed-dispersion arc (as it matches from the defined optics of the stochastic injection straight to a zero-dispersion section), it need not preserve optical symmetry and we find an optimised configuration for four quadrupoles. The strength and spacing of the quadrupoles is set based on matching the dispersion conditions at the arc's start and end, whilst minimising transverse beam size. As long as the horizontal beam size in the second arc is kept below the maximum horizontal beam size achieved in the first arc (which is as low as achievable), the arc will not impose any additional limitations on the horizontal acceptance. The vertical beam size is maintained below the 400 mm diameter assumed as the quadrupole aperture.

3.6 Design of Dispersion-Suppressed Straight

With the layout of the target station and injection-matching arcs of the transfer line fixed, the remaining parameters of the transfer line can be fixed. The positioning of the target station arc and its bending angle is fixed, as is the value of α and the bending angle of the injection-matching arc and the stochastic injection section. The dimensions of these sections are also fixed. Hence, the remaining parameters to determine are the length of the dispersion-

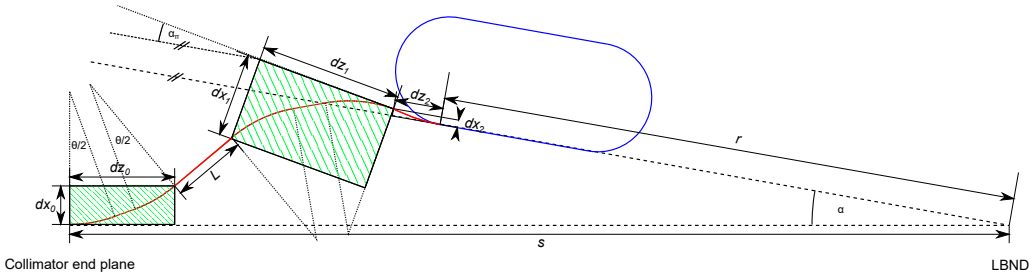

Figure 8: Simplified geometry of the system, not drawn to scale. The shaded areas represent the target station arc and the injection-matching arc, and the trajectory of pions is depicted in red. The LEnuSTORM ring is drawn in blue. The left hand side of the image represents the end plane of the target station collimator, whilst the long baseline near detector is positioned at the right.

suppressed straight within the transfer line L, and the distance of ring origin point along the axis of the production straight r (Figure 8). The constraints on these parameters can be expressed - in terms of quantities shown in Figure 8 - as:

$$dx_2 \cos\alpha + dz_2 \sin\alpha + r \sin\alpha = L \sin\theta + dx_1 \cos\alpha_\pi - dz_1 \sin\alpha_\pi + dx_0, \quad (2)$$

$$dz_2 \cos\alpha - dx_2 \sin\alpha + s - r \cos\alpha = L \cos\theta + dz_1 \cos\alpha_\pi + dx_1 \sin\alpha_\pi + dz_0. \quad (3)$$

This system can be solved simultaneously to obtain the values for r and L which minimise the line length assuming the specified arcs at the target station and injection point. Quadrupoles are then positioned in this straight, and their strengths and spacing are optimised to match the Courant-Snyder parameters at the exist of the target station arc to those at the entrance of the injection-matching arc.

3.7 Final line design & performance

The optics of the T2R line are depicted in Figure 9 (Left). The projections of the beams onto the transverse axes x and y are shown in Figure 9 (Right), assuming the 50% emittance value from 2 and a momentum spread of $\pm$10%.

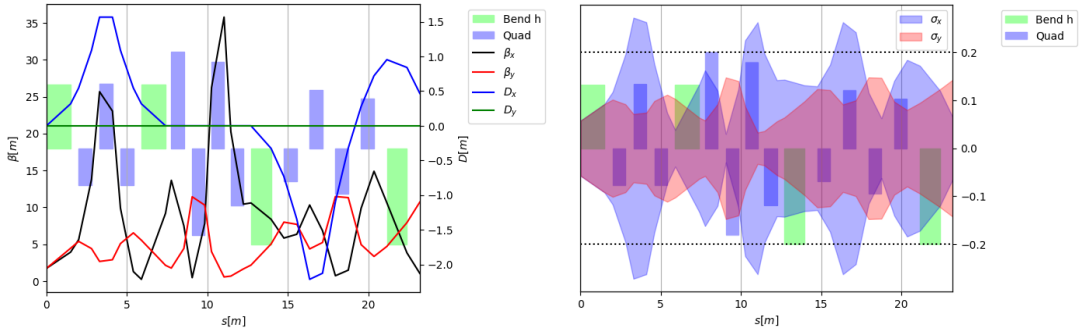

Figure 9: Linear optics of the full transfer line from the collimator end plane to the injection septum of the LEnuSTORM ring (Left). Projection of the design beam onto the transverse axes. The assumed magnet apertures are shown with dashed horizontal lines (Right).

With the assumed magnet aperture of $\pm$20 cm in each plane, the full beam is accepted in the vertical plane. It can be seen that the assumed design beam exceeds the aperture in the horizontal plane at the midpoint of the first arc - this is an unavoidable consequence of the constraints on magnet spacing in the first arc. This is the maximum in the transverse beam size, and all subsequent transverse beam size peaks are maintained below this value.

Tracking of the pion distribution was performed using Xsuite. The transverse phase space distributions at the end of the line (at the injection septum of the LEnuSTORM ring) are shown in Figure 10.

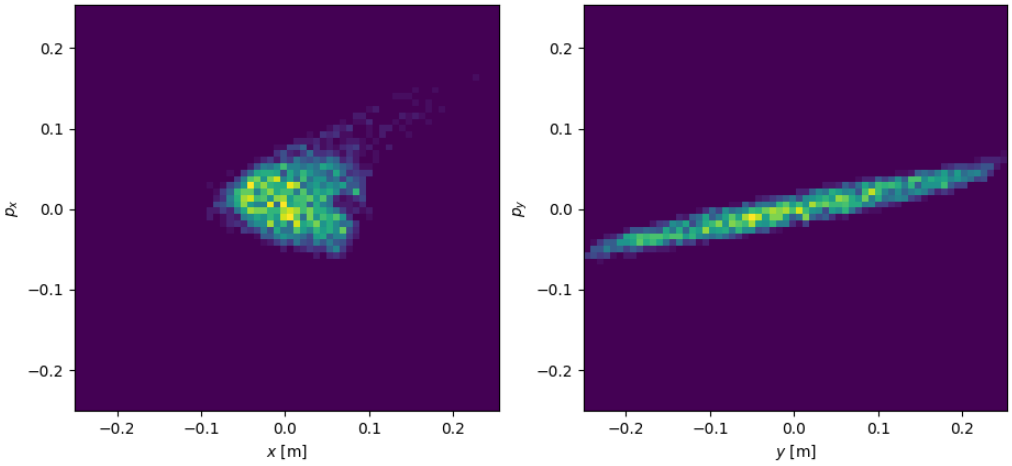

Figure 10: Transverse phase space of the pion beam at the injection point.

The longitudinal momentum spectra of surviving pions are displayed in Figures 11 (Left) and 11 (Right). The fraction of pions in the input distribution transmitted through the collimator is 15.1% whilst the fraction of the pions transmitted through the entire collimator-transfer line assembly is 0.113%. The efficiency of the line can be expressed as the ratio of the pions at the downstream plane of the collimator, within the design momentum range of ±10%, to the pion count at the injection point of the LEnuSTORM ring. This gives a value of 10.8%. Overall, this corresponds to a rate of 1.881×10^{-4} injected pions per proton on target.

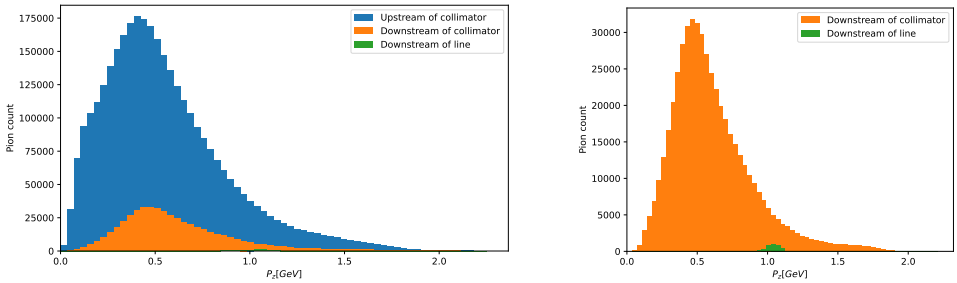

Figure 11: Momentum distribution of pions upstream of the collimator, downstream of the collimator, and downstream of the transfer line (Left). Distribution of pions at the end plane of the collimator and at the end point of the transfer line (Right).

A final optimisation of performance should be performed numerically using a detailed end-to-end tracking simulation once field maps for all elements are available and the ring design is finalised, with the muon count at the end of the production straight as the target variable. Further tuning of quadrupole strengths and positioning may then yield small improvements in rate by better accounting for nonlinear effects and the details of fringe field effects that have not been taken into account by this study.

4 Summary

This document outlines the design of the transfer line and the principles under which it has been designed, such that modifications for future changes to the facility layout can be accommodated. The performance of the transfer line is evaluated, assuming an initial pion distribution given by a FLUKA simulation of the target and horn. The final rate of pions arriving at the injection septum of the LEnuSTORM ring is 1.881×10^{-4} per proton on target which exceeds the anticipated value of 1.0×10^{-4} used for the neutrino flux estimation in [7]. A final tuning of line parameters should be made with an end-to-end tracking simulation once ring parameters are finalised and realistic magnet field maps are available. This may yield some small improvements in the total rate. Nonetheless, the current performance is within acceptable bounds for the study.

References

[1] ESSnuSB+ WP3. D3.2, design of the pion extraction and focusing systems, 2025.

[2] COMSOL Multiphysics® v. 5.4., 2024.

[3] C. Ahdida et al. New Capabilities of the FLUKA Multi-Purpose Code. *Front. in Phys.*, 9:788253, 2022.

[4] Vasilis Vlachoudis. FLAIR: A powerful but user friendly graphical interface for FLUKA. In *International Conference on Mathematics, Computational Methods & Reactor Physics 2009*, pages 790–800, 2009.

[5] Giovanni Iadarola et al. Xsuite: An Integrated Beam Physics Simulation Framework. *JACoW*, HB2023:TUA2I1, 2024.

[6] F. Bordry, L. Bottura, A. Milanese, D. Tommasini, E. Jensen, Ph. Lebrun, L. Tavian, J. P. Burnet, M. Cerqueira Bastos, V. Baglin, J. M. Jimenez, R. Jones, T. Lefevre, H. Schmickler, M. J. Barnes, J. Borburgh, V. Mertens, R. W. Aβmann, S. Redaelli, and D. Missiaen. *Accelerator Engineering and Technology: Accelerator Technology*, pages 337–517. Springer International Publishing, Cham, 2020.

[7] Milestone MS21+ : First estimate of the neutrino flux from LEnuSTORM, 2025.